Circulation Research

ORIGINAL RESEARCH

In Situ Expansion, Differentiation, and Electromechanical Coupling of Human Cardiac Muscle in a 3D Bioprinted, Chambered Organoid

Molly E. Kupfer,* Wei-Han Lin,* Vasanth Ravikumar, Kaiyan Qiu, Lu Wang, Ling Gao, Didarul B. Bhuiyan, Megan Lenz, Jeffrey Ai, Ryan R. Mahutga, DeWayne Townsend, Jianyi Zhang, Michael C. McAlpine, Elena G. Tolkacheva, Brenda M. Ogle

RATIONALE: One goal of cardiac tissue engineering is the generation of a living, human pump in vitro that could replace animal models and eventually serve as an in vivo therapeutic. Models that replicate the geometrically complex structure of the heart, harboring chambers and large vessels with soft biomaterials, can be achieved using 3-dimensional bioprinting. Yet, inclusion of contiguous, living muscle to support pump function has not been achieved. This is largely due to the challenge of attaining high densities of cardiomyocytes—a notoriously nonproliferative cell type. An alternative strategy is to print with human induced pluripotent stem cells, which can proliferate to high densities and fill tissue spaces, and subsequently differentiate them into cardiomyocytes in situ.

OBJECTIVE: To develop a bioink capable of promoting human induced pluripotent stem cell proliferation and cardiomyocyte differentiation to 3-dimensionally print electromechanically functional, chambered organoids composed of contiguous cardiac muscle.

METHODS AND RESULTS: We optimized a photo-crosslinkable formulation of native ECM (extracellular matrix) proteins and used this bioink to 3-dimensionally print human induced pluripotent stem cell–laden structures with 2 chambers and a vessel inlet and outlet. After human induced pluripotent stem cells proliferated to a sufficient density, we differentiated the cells within the structure and demonstrated function of the resultant human chambered muscle pump. Human chambered muscle pumps demonstrated macroscale beating and continuous action potential propagation with responsiveness to drugs and pacing. The connected chambers allowed for perfusion and enabled replication of pressure/volume relationships fundamental to the study of heart function and remodeling with health and disease.

CONCLUSIONS: This advance represents a critical step toward generating macroscale tissues, akin to aggregate-based organoids, but with the critical advantage of harboring geometric structures essential to the pump function of cardiac muscle. Looking forward, human chambered organoids of this type might also serve as a test bed for cardiac medical devices and eventually lead to therapeutic tissue grafting.

GRAPHICAL ABSTRACT: A graphical abstract is available for this article.

Key Words: biocompatible materials ■ bioprinting ■ extracellular matrix proteins ■ induced pluripotent stem cells ■ myocytes, cardiac ■ organoids ■ tissue engineering

Human cardiac muscle derived ex vivo is in high demand as a substrate for testing drug efficacy and toxicity, as an analog for studying tissue remodeling associated with cardiac muscle damage or disease, and as a prelude to clinical cardiac repair. The field of cardiac tissue engineering seeks to produce such tissue models by capitalizing on

Novelty and Significance

What Is Known?

- Engineered cardiac tissues enable drug testing and disease modeling using human cells, but many of these tissues lack the geometric complexity and pumping capacity of the native heart.
- Three-dimensional (3D) bioprinting provides a means to fabricate geometrically complex, cell-laden structures using soft biomaterials including extracellular matrix proteins that are critical to cell viability and function.
- Cardiomyocytes have a low proliferative capacity, which makes it challenging to achieve the high cell densities needed to produce contiguous muscle function in a 3D structure.

What New Information Does This Article Contribute?

- We have developed a photo-crosslinkable bioink formulation composed of extracellular matrix proteins, which can be 3D printed into complex geometries and enables robust expansion and subsequent in situ differentiation of human pluripotent stem cells into cardiac muscle.
- Human stem cell–laden bioink is 3D printed to generate a perfusable structure based on the geometry of the human heart, after which cells are allowed to proliferate to high densities before differentiation.
- The resulting human chambered muscle pump exhibits thick and contiguous muscularization, electrical connectivity, and pump function that manifests in measurable changes in pressure and volume.

This article demonstrates the use of 3D bioprinting to fabricate perfusable, chambered heart mimics possessing large vessel conduits and a septal throughway to enable continuous, unidirectional flow. One of the primary barriers to generating cardiac tissues in vitro is that cardiomyocytes rarely proliferate or migrate, making it difficult to fill tissue gaps and achieve thick layers of contiguous muscle. We have overcome this hurdle by printing with human induced pluripotent stem cells instead of cardiomyocytes. A custom, extracellular matrix–based bioink formulation enables stem cells to proliferate to high densities before induction of cardiac differentiation, thus allowing the cells to form robust connections to each other as they differentiate. The result is a synchronously contracting human chambered muscle pump with wall thicknesses of up to half a millimeter and cell densities on the same order of magnitude as native cardiac tissue. Human chambered muscle pumps exhibit continuous action potential propagation, responsiveness to pharmacological agents and electrical pacing, and measurable changes in pressure and volume with contraction. In the future, this model could be used as a test bed for a variety of drugs and devices, as well as a model for genetic diseases that manifest in altered pressure-volume dynamics.

Nonstandard Abbreviations and Acronyms

αSMA	alpha-smooth muscle actin
3D	3 dimensional
Bin1	bridging integrator-1
CD31	cluster of differentiation 31
ColMA	collagen methacrylate
cTnI	cardiac troponin I
cTnT	cardiac troponin T
Cx43	connexin 43
DDR2	discoidin domain receptor 2
ECM	extracellular matrix
ERK	extracellular signal-related kinase
FN	fibronectin
GelMA	gelatin methacrylate
GSK3β	glycogen synthase kinase 3 beta
hChaMP	human chambered muscle pump
hiPSC	human induced pluripotent stem cell
ILK	integrin-linked kinase
Ki67	nuclear antigen Ki67
LAP	lithium phenyl-2,4,6-trimethylbenzoylphosphinate
LN	laminin-111
MEK	mitogen-activated protein kinase
MMP	matrix metalloproteinase
RyR2	ryanodine receptor 2
SERCA2a	sarcoplasmic reticulum ATPase2a

the capacity of stem cells to differentiate to all cardiac cell types, of biomaterials to direct cardiac cell behavior, and of 3-dimensional (3D) fabrication technologies to use biologic materials. Early engineered heart tissues consisted of geometrically simple structures (strips or rings) made by casting cardiomyocytes in an ECM (extracellular matrix)-based gel.[1–3] These types of tissues are very useful because they can be attached to rigid or flexible posts to provide resistance against which the tissue can contract and to modulate mechanical loading.[4,5] At the same time, the lack of geometric complexity limits the utility of the model for in

vitro study of cardiac function and disease, as these tissues can generate force but do not pump fluid. To address this issue, researchers have made strides in the generation of volume-handling cardiac tissue models capable of recapitulating pressure-volume dynamics of the heart.[6–8] However, these tissues are limited to a single ventricle model and thus lack the capacity for perfusion. Indeed, multiple existing single ventricle models rely on their simple cup-like geometry to enable casting of a cardiomyocyte-laden gel[6] or seeding of cardiomyocytes after fabrication.[7] These methods are suitable for an open, single-chamber structure that is wider on top than at the base; however, to generate an enclosed, perfusable model, more advanced fabrication technologies are required.

3D bioprinting has been proposed as a means to generate more geometrically complex tissues from the bottom-up. The concept is gaining traction, as the ability to print cell-laden tissues composed entirely of native proteins or biocompatible synthetic components is possible and accessible to many laboratories.[9–17] Multiple studies have demonstrated the capacity to print entire heart organ models using biological materials, but the resulting constructs have either lacked cells[8,9] or evidence of electromechanical function.[18] The fact that macroscale contractile function has not yet been achieved in a 3D printed, perfusable, chambered heart model reflects the challenges associated with handling mature cardiac muscle cells.

More specifically, cardiomyocytes do not proliferate or migrate readily. For this reason, it is challenging to achieve the high cell density required for the formation of functional cell-cell junctions while maintaining the structural support needed for an enclosed chamber. In fact, the only 3D printed, volume-holding structure to successfully demonstrate cardiac function is a single ventricle model. Specifically, Lee et al[8] printed a support material (ie, type I collagen) as a shell that is filled with cardiomyocytes in a fibrinogen suspension at a concentration of 300 million cells/mL. The electrophysiological function demonstrated by Lee et al in the printed ventricle mimic is extremely exciting; however, using the print methodology described, it would be difficult to attain more complicated, enclosed structures. In addition, it is technically challenging to generate such a large number of cardiomyocytes that sustain viability and the capacity to organize with transfer from dish to 3D printed structure. This process requires the disruption of previously formed cell-cell connections, and a cell strainer is required to remove aggregated cardiomyocytes, which further adds to the total number of cardiomyocytes that must be produced before printing. An alternative approach described here is to print stem cells, which are highly proliferative, and then induce differentiation of cardiomyocytes in situ following cell expansion.

To enable this approach, we sought to develop a bioink formulation that (1) promotes human induced pluripotent stem cell (hiPSC) viability, (2) enables hiPSC proliferation and subsequent differentiation into cardiomyocytes, and (3) is amenable to printing complex structures in a gelatin microparticle bath without requiring any further support structure or mold. To support proliferation, the bioink must be porous and susceptible to degradation such that stem cell colonies can easily expand. To support differentiation, the bioink should ideally contain integrin-binding motifs that enhance signaling associated with cardiomyocyte-specific differentiation. There is now clear evidence from our group and the work of others that stem cell maturation and differentiation and the proper function of cells derived thereof are critically dependent on the temporal and spatial engagement of cell surface integrins with ECMs both in a given organ system during development[19] and in the context of ex vivo stem cell culture.[20–27] As one of many examples, mesoderm specification has been linked to $\alpha5\beta1$ integrin activation. Engagement of this integrin by ECM (especially LN [laminin]-511/111 and FN [fibronectin]) modulates BMP4 (bone morphogenetic protein 4) expression, which together with Wnt, fibroblast growth factor, and transforming growth factor-β/nodal/activin signaling mediates differentiation to mesoderm.[26] In addition, engagement of fibroblast-derived ECM via β1, α2, and α3 integrins in human embryonic stem cells activates the Wnt/β-catenin pathway via the MEK (mitogen-activated protein kinase)-ERK (extracellular signal-related kinase) pathway, which drives endoderm differentiation.[28] Finally, FN/integrin β1/β—catenin signaling promotes the emergence of mesoderm from induced pluripotent stem cells. This study was the first to establish a direct link between elements of the focal adhesion, namely ILK (integrin-linked kinase), with GSK3β (glycogen synthase kinase 3 beta)[29]—the primary antagonist of β-catenin.

In this work, we build on our understanding of ECM engagement and stem cell differentiation by tapping our already developed, optimized ECM formulation to promote cardiomyocyte differentiation[30] and incorporate this formulation into a bioink that is conducive to hiPSC proliferation and can be deposited with spatial fidelity. The end result is a living pump that mimics the chambers and large vessel conduits of a native heart while housing viable, densely packed, and functional cardiomyocytes (Figure 1). These human chambered muscle pumps (hChaMPs) can be maintained long term (≥6 weeks) and will pave the way for generating increasingly complex structures that could include spatially designated pacemaker cells and an associated conduction system, an epicardium to support remodeling with health, injury, or disease, as well as a host of other important attributes including an arterial and venous nutrient exchange system.

METHODS

The authors declare that all supporting data are available within the article and the associated Data Supplement unless otherwise specified. For data not shown, findings are available from the corresponding authors upon reasonable request. A
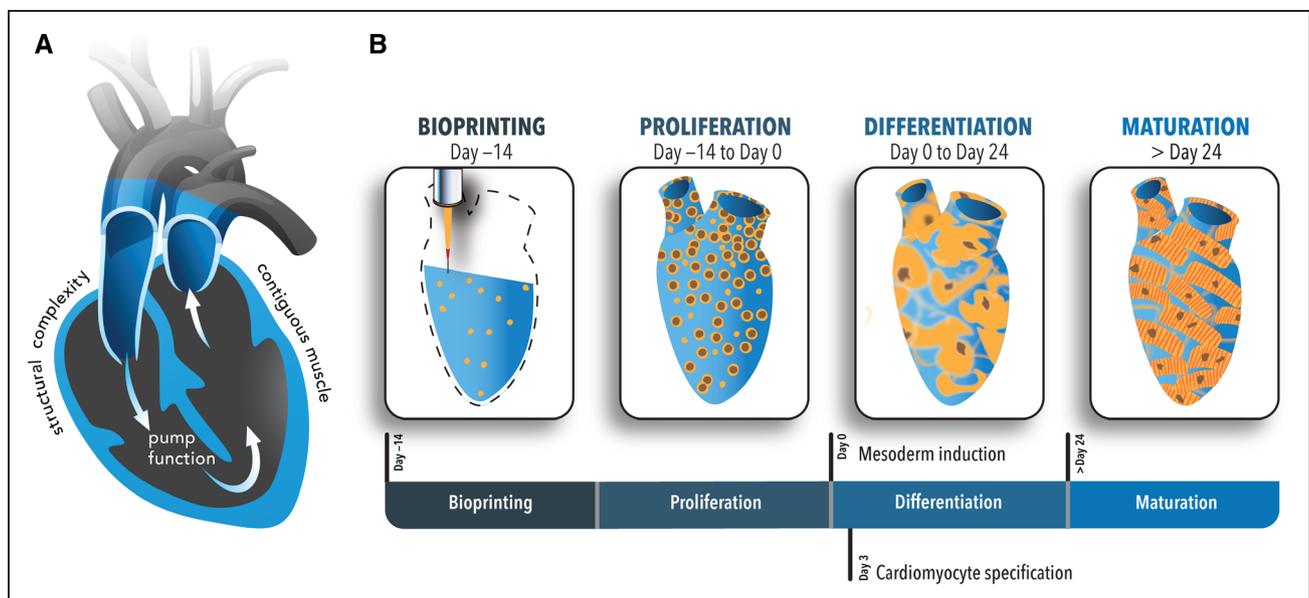
Figure 1. Graphical abstract.
A, Cross-sectional view of the design template for the human chambered cardiac pump (hChaMP). The template was derived from a magnetic resonance imaging scan of the human heart that was reduced in scale 10× (1.3 cm at its longest axis, akin to the size of a murine heart) and modified to harbor a 1-way flow loop through the chambers of the heart template. The goal was to create a geometrically complex cardiac tissue with contiguous muscle and associated pump function. **B**, The panels designate the unique organoid-like approach to generate the hChaMP wherein human induced pluripotent cells (hiPSCs) were deposited with an optimized, ECM-based bioink that allowed for expansion of the hiPSCs to attain tissue-like densities and subsequent differentiation to cardiomyocytes. Over time, the hChaMP could beat synchronously, build pressure, and move fluid akin to a living pump.

detailed description of the methodology can be found in the Data Supplement. Please also see the Major Resources Table in the Data Supplement.

RESULTS

Optimization of a Bioink Supportive of hiPSC Proliferation and Differentiation

We previously identified a formulation of ECM proteins that optimally supports the differentiation of cardiomyocytes from induced pluripotent stem cells.[30] We thus began a similar optimization study here to identify an ECM-based bioink to support the generation of geometrically complex cardiac tissue. The design criteria included printability to support extrusion from a 27-gauge needle resulting in a submillimeter linewidth resolution (630.6±54.2 µm, n=10), easy material handling of the printed structure, the capacity to support proliferation of hiPSCs incorporated directly into the bioink, and the ability to support cardiomyocyte differentiation of said hiPSCs. We began with a gelatin methacrylate (GelMA) base material to be cross-linked via photoactivation with lithium phenyl-2,4,6-trimethylbenzoylphosphinate (LAP) to accomplish printability requirements and avoid inclusion of synthetic support materials. Material handling was difficult below 10% GelMA as final structures were flimsy and easily damaged, whereas printability was difficult to accomplish above 15% GelMA as extrusion required

high pressures, which made material control difficult and which sometimes resulted in cell damage. Thus, the optimization matrix contained either 10% (100 mg/mL) or 15% (150 mg/mL) GelMA. To the GelMA, we added hiPSCs and ECM proteins critical to support cardiomyocyte differentiation in prior work,[30] namely FN, LN-111, and collagen methacrylate (ColMA) ranging from 0 to 190 µg/mL, 0 to 190 µg/mL, and 0% to 0.5% (or 0−5 mg/mL), respectively (Figure 2A). FN and LN were added in equal amounts for all conditions, with the concentration scaled to the ColMA concentration (38 µg/mL FN and LN with 0.1% ColMA, 95 µg/mL FN and LN with 0.25% ColMA, and 190 µg/mL FN and LN with 0.5% ColMA). All conditions are annotated with GelMA (G) concentration, ColMA (C) concentration, and the presence of the corresponding amounts of FN and LN. For example, 10G0.10CFL refers to a bioink consisting of 10% GelMA and 0.10% ColMA, supplemented with FN and LN. Ease of material handling was assessed via measurement of viscosity before printing (Table). We found, according to design, that all of the ink formulations fell within the range of 10 to 40 cP, ensuring low pressure requirements (28−38 kPa) with printing. Ability to support hiPSC health was assessed via measurement of cell area in the printed structure at day −13 as an indicator of cell viability and colony area at day 0 as an indicator of proliferation with continued cell health (Table; Figure 2B and 2C). We found that viability was relatively consistent across all formulations at day −13 with the exception
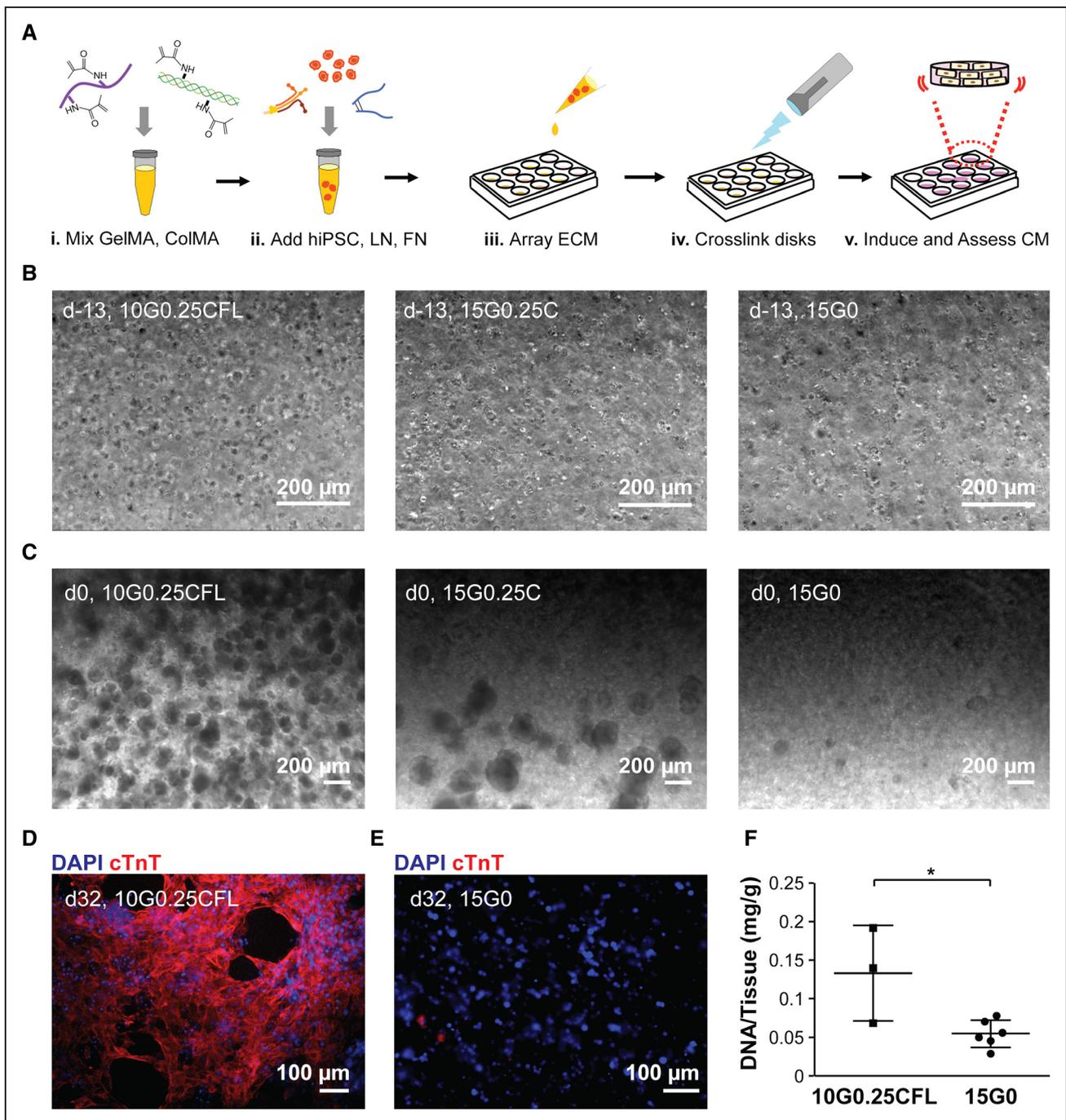
Figure 2. Optimization of an ECM (extracellular matrix)-based bioink for printing geometrically complex cardiac structures.
A, Bioink formulations delineated in the Table were combined with human induced pluripotent cells (hiPSCs) and pipetted into wells to form gels. **B**, Representative images of single cells in 3 bioink formulations at day −13: 10G0.25CFL, 15G0.25C, and 15G0. **C**, Representative images of good (10G0.25CFL), fair (15G0.25C), and poor (15G0) proliferation based on colony area at day 0. **D**, A representative image of good (10G0.25CFL) cardiomyocyte (CM) differentiation at day 32. **E**, A representative image of poor (15G0) CM differentiation at day 32. **F**, DNA content of the disks with good (10G0.25CFL) versus poor (15G0) CM differentiation. n=3 disks for 10G0.25CFL, and n=6 disks for 15G0. *$P<0.05$ compared with 15G0, Student t test. ColMA indicates collagen methacrylate; cTnT, cardiac troponin T; DAPI, 4′,6-diamidino-2-phenylindole; FN, fibronectin; GelMA, gelatin methacrylate; and LN, laminin-111.

of the ink composed exclusively of 15% GelMA. However, proliferation varied substantially across formulations with those gels containing 10% GelMA generally exceeding those with 15% GelMA. Specific formulations 10G0.25CFL, 10G0.50CFL, and 10G0.10C supported

the highest levels of proliferation (range, 55.2%–61.8% colony area). The ability to support hiPSC differentiation to cardiomyocytes was assessed via measurement of cTnT (cardiac troponin T). We found that differentiation outcomes not only corresponded to the GelMA fraction

Table. Design Criteria for Bioink With Outcomes Associated With a Given Formulation

Formulation*	Viscosity (d−15), cP	Cell Area (d−13), %	Colony Area (d0), %	Differentiation (d32), %cTnT+	Beating† (0–3)
10G0.10CFL	14.3	21.8±1.9‡	52.0±3.4	46.6±23.9‡	2.8‡
10G0.25CFL§	14.7	21.6±2.9‡	57.6±7.4‡	67.9±6.6‡	2.8‡
10G0.50CFL	15.9	20.3±0.7	61.8±3.4‡	17.2±29.8	1.6
15G0.10CFL	34.2	20.9±2.0	32.2±21.4	11.2±17.4	0.8
15G0.25CFL	34.9	23.3±0.4‡	55.0±7.6	23.7±16.2	2.0
15G0.50CFL	35.6	21.3±1.9	54.1±9.0	35.4±6.4	2.8‡
10G0.10C	9.6	17.3±1.3	55.2±4.3‡	38.2±11.3	2.5
10G0.25C	11.0	16.8±0.2	53.5±4.4	44.4±7.0	2.8‡
10G0.50C	11.9	18.9±0.6	55.0±3.1	42.3±1.6.9	2.2
15G0.10C	19.6	19.2±2.5	16.2±11.5	0.2±0.5	0.1
15G0.25C	23.7	20.0±1.4	38.2±7.3	4.4±6.0	0.5
15G0.50C	24.1	17.2±1.7	21.0±19.7	0±0	0
10G0	11.6	20.6±0.8	51.1±2.7	43.5±4.5‡	2.9‡
15G0	18.2	14.7±1.3	9.2±3.8	0.1±0.1	0

cTnT indicates cardiac troponin T; and d, day.

*C indicates collagen methacrylate; F, fibronectin; G, gelatin methacrylate; and L, laminin-111. Numbers preceding letters indicate percentage.

†Beating scale was assessed by grading the contractile performance visually from 0 (no beating) to 3 (best beating).

‡Highest values.

§Optimum bioink formulation.

but also were largely dependent on the addition of FN and LN (Table; Figure 2D and 2E). Specific formulations 10G0.10CFL, 10G0.25CFL, and 10G0.25C supported the highest levels of differentiation. There was only one formulation that ranked in the top 3 for all criteria, 10G0.25CFL or 100 mg/mL GelMA, 2.5 mg/mL ColMA, 95 µg/mL FN, 95 µg/mL LN-III, and 5 mg/mL LAP. For the cross-linked gels of this specific formulation, the storage modulus (G′, 6.14±1.13 kPa) was ≈2 orders of magnitude higher than the loss modulus (G″, 0.09±0.06 kPa; Figure I in the Data Supplement), suggesting the elastic nature of the gels with a stiffness similar to that of the late embryonic heart.[31] In addition, this formulation achieved a cell density of 0.1 mg DNA/g of gel, which is on the same order of magnitude of native cardiac tissue (≈0.3 mg DNA/g of myocardial mass) and significantly higher than the condition that produced the lowest amount of differentiation[32] (Figure 2F). Thus, it was this formulation that was used for all subsequent studies.

Bioprinted Chambered Cardiac Mimic With Large Vessel Extensions Exhibits High Fidelity to the Digital Template

The optimized bioink could be extruded from a needle, but the bioink was of low relative viscosity (14.7 cP), and so the ability to fabricate structures beyond simple stacking geometries was challenging with standard extrusion modalities in air. To address this hurdle, we developed an approach that involved backfilling an inverted geometry made of sacrificial ink; however, low cell viability and low proliferation associated with the sacrificial ink limited

further use (Figure II in the Data Supplement; Movies I and II in the Data Supplement). Ultimately, we used free-form reversible embedding of suspended hydrogels[9,12] with success, wherein our embedding material or slurry consisted of gelatin microparticles. This bioprinting approach was used for the remainder of the study. The digital print template was derived from a magnetic resonance imaging scan of a human heart that was scaled to the size of a murine heart such that the longest axis was ≈1.3 cm. In addition, the septum between ventricles was partially removed to provide a throughway such that unidirectional flow could be propagated through the printed structure for ease of nutrient delivery. The structure was further modified to limit the vascular connections to 2 major vessels extending from the top of the structure, corresponding to aorta and vena cava from the digital template. The size of the gelatin particles was most critical among print parameters for attaining feature sizes necessary to replicate the chambered cardiac mimic. We found that the size of gelatin microparticles scaled inversely with the resolution of the print (Figure III in the Data Supplement). Particles of ≈100 µm could support printing of the chambered cardiac mimic with intact chambers, patent large vessels, and material properties conducive to handling (Movie III in the Data Supplement). Magnetic resonance imaging scans of the bioprinted structures show intact chambers (Figure IV in the Data Supplement), and volumetric 3D digital reconstructions of the bioprinted cardiac mimic were compared with the volumetric 3D digital template using CloudCompare 2.10.2 software (www.cloudcompare. org). A qualitative, cross-sectional comparison showed a

high level of fidelity of the interior chambers (Figure 3A), which was substantiated quantitatively via generation of a distance map from the overlaid template and printed structure (Figure 3B and 3C). The fraction of voxels of the printed structure within 0.5 mm of the template was found to be 86%. Further, polyethylene tubing and fluorinated ethylene propylene could be securely attached to the printed structure using tissue adhesive, and inclusion of dye in the perfusate showed intact and perfusable chambers in the interior space of the bioprinted, chambered cardiac mimic (Figure 3D; Movie IV in the Data Supplement).

hiPSCs 3D Printed in an Optimized Bioink Give Rise to a Contiguous Muscle Wall to Form a hChaMP

To determine whether human pluripotent stem cells could proliferate to populate the entire hChaMP, hiPSCs were included during the print using the optimized bioink formulation (Figure 3E). Given the imaging complexity of counting individual cells in such a large construct, we instead quantified colony size in at least 4 randomly chosen regions of 8 different hChaMPs at 2 weeks in culture. By day 14, ≈90% of the bioink volume was populated with cells, both singular and in large colonies, with
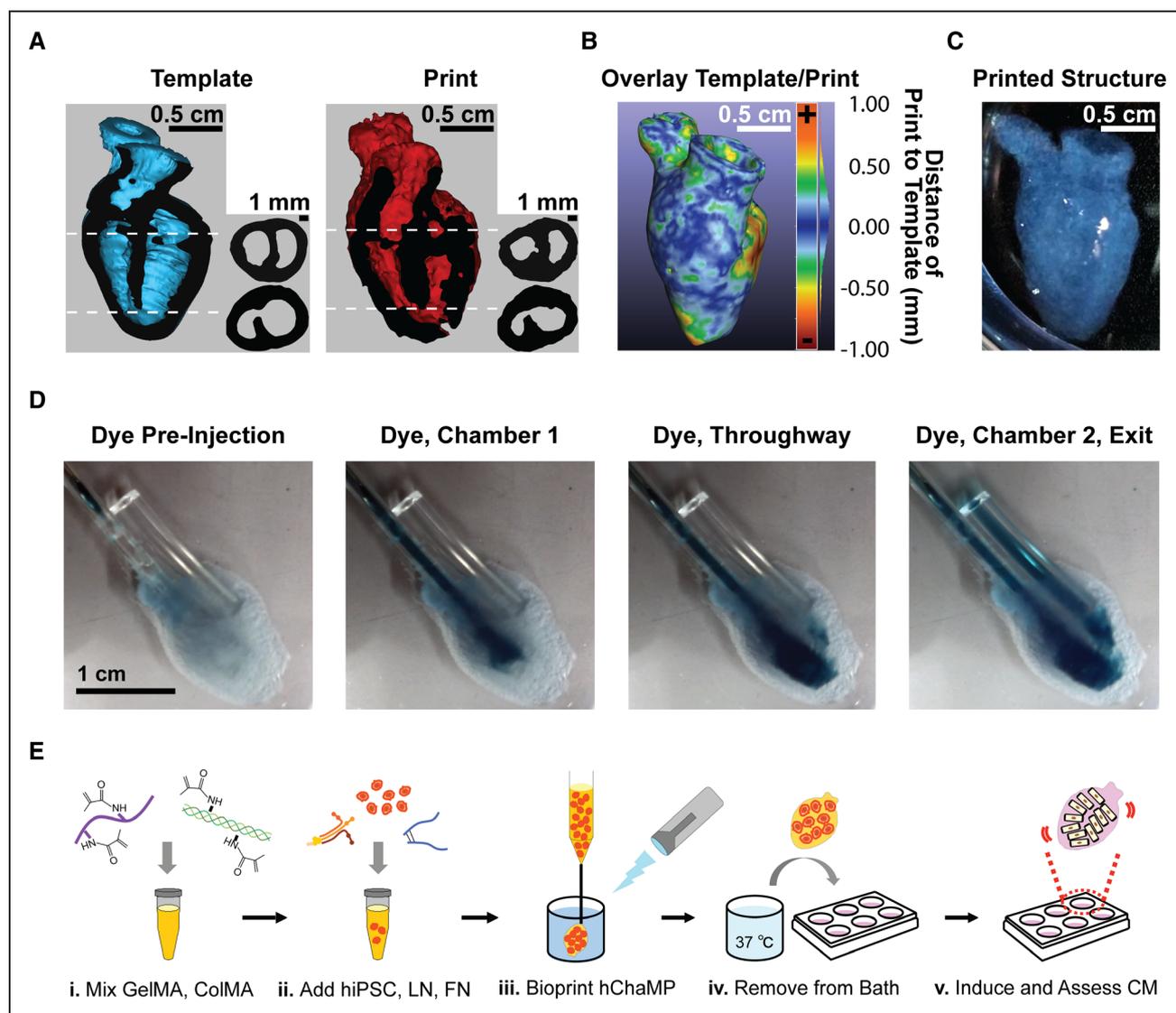

Figure 3. Bioprinting of optimized bioink yields chambered geometry with discrete vessels that act as perfusion conduits.
A, Three-dimensional (3D) digital models of the intact human heart (template) or 3D printed structure (print). Longitudinal cutaway view of template (blue) and print (red) with cut surface (black). Next to each cutaway is a cross-sectional view of template and print at 2 different regions, one featuring the intact septum and the other featuring the septal throughway, as indicated by the dotted lines. **B**, A heat map showing the geometric difference between the template and the print; scale, +1.0 to −1.0 mm from the template. **C**, A photograph of a printed, chambered construct. **D**, Image series taken from Movie IV in the Data Supplement showing perfusion of the bioprinted cardiac mimic. The scale is the same for each image. **E**, The optimized bioink formulation was combined with human induced pluripotent cells (hiPSCs) and bioprinted to form a human chambered muscle pump (hChaMP). CM indicates cardiomyocyte; ColMA, collagen methacrylate; FN, fibronectin; GelMA, gelatin methacrylate; and LN, laminin-111.

40±11% corresponding to colony area (Figure 4A). It was at this point that a cardiomyocyte differentiation protocol was imposed (Figure 1). Six weeks following lactate purification, cells of hChaMPs were again probed for proliferation, this time via expression of Ki67 (nuclear antigen Ki67); we found that 25.6±3.1% of cells are proliferative at this stage (Figure 4B). At the same time point, cell death was assessed via terminal deoxynucleotidyl transferase dUTP nick end labeling and showed very limited cell death (5.7±0.6% terminal deoxynucleotidyl transferase dUTP nick end labeling–positive cells), suggesting ongoing cell health in the hChaMP (Figure 4C).

To determine whether hiPSCs could undergo efficient differentiation to cardiomyocytes in the hChaMP and thereby form a contiguous muscle volume, hChaMPs were stained for sarcomeric protein, cTnI (cardiac troponin I). We determined that 87.6±4.9% of the cells of the structure were cardiomyocytes according to expression of cTnI (Figure 4D). We also probed for evidence of other cardiac cell types, since mesoderm induction could have been followed by differentiation to cardiac fibroblasts, endothelium, or smooth muscle cells. We found no compelling evidence of cardiac fibroblasts (via staining for DDR2 [discoidin domain receptor 2], data not shown), but smooth muscle cells (10.5±4.2% of cells via staining for αSMA [alpha-smooth muscle actin]) and endothelial cells (4.2±2.4% of cells via staining for CD31 [cluster of differentiation 31]) were present in hChaMPs. Importantly, the combined cardiac cell cocktail often fully circumvented the hChaMP (Figure 4E), and the thickness of the wall was typically between 100 and 500 μm with the thickest region exceeding 500 μm (Figure 4E). The majority of the cells at 6 weeks following lactate purification were associated with the outer portion of the hChaMP wall. Bioink could be discerned in the inner portion of the hChaMP wall but was largely without cells (Figure 4E, white oval).

hChaMPs Express and Localize Proteins Consistent With a Maturing Cardiomyocyte Phenotype

hChaMPs were cultured for at least 6 weeks following completion of the differentiation and lactate purification protocols. Before extended culture, hChaMPs were transitioned from static cultures to convective environments wherein nutrient exchange might be better achieved via rocking. hChaMPs were neither perfused in a bioreactor, exposed to controlled, resistive mechanical stimulation, nor exposed to electrical stimulation; all factors shown to improve maturation. Even so, robust expression of gap junction protein Cx43 (connexin 43) was found in substantive plaques between adjacent cardiomyocytes (1.90±0.12% of α-actinin area). Also at the cell surface, inward rectifying potassium channel Kir2.1,

expressed in fetal and adult cardiomyocytes to stabilize the resting membrane potential, was detected at high levels (1.84±0.11% of cTnI area; Figure 5A and 5B). Intracellular machinery associated with the sarcolemma and sarcoplasmic reticulum was also well expressed and appropriately organized (Figure 5C). In particular, the membrane scaffolding protein Bin1 (bridging integrator-1) was found in positive striations along myofibrils (1.43±0.08% of α-actinin area). SERCA2a (sarcoplasmic reticulum ATPase2a) exhibited signal in the majority of cells, with staining in close apposition to the myofibrils (1.50±0.19% of cTnT area). Similarly, RyR2 (ryanodine receptor 2) formed a ladder-like and regular network along the myofibril (1.48±0.05% of α-actinin area) with greater regularity than that observed in cardiomyocytes derived in a 2-dimensional monolayer at similar time points following differentiation, suggestive of advanced maturation in the hChaMP.

hChaMPs Exhibit Contiguous Electrical Function and Pump Dynamics

hChaMPs could be routinely fabricated such that macroscale beating was observed (Movie V in the Data Supplement). To determine the extent to which electromechanical function was preserved throughout the hChaMP, electrical function was first measured via calcium transients of randomly selected regions of hChaMPs (week 2, n=4 hChaMPs; week 6, n=3 hChaMPs; n=14–21 regions per hChaMP; Figure 6A). Calcium transients were measured at both 2 and 6 weeks after cessation of the differentiation and purification protocols to determine dynamics of calcium handling over time. Peak amplitude did not change over time nor did beating frequency calculated from calcium peaks, suggesting that the degree of maturation had largely been achieved by 2 weeks and that health of the hChaMP could be maintained for at least 6 weeks. Calcium handling could be increased in frequency with the addition of isoproterenol, a nonselective β-adrenoreceptor agonist, and could be decreased in amplitude with the addition of verapamil, a phenylalkylamine calcium channel blocking agent, thus supporting the capacity of the hChaMP to appropriately respond to drug stimuli (Figure 6B). In addition, a dose-response curve was generated from calcium transient data to examine the effect of isoproterenol concentration on beat rate (Figure 6C). From this curve, the isoproterenol concentration that produced 50% of the maximum response was determined to be 0.009 μM, which is very similar to what has been previously reported for stem cell–derived cardiomyocytes.[33]

Optical mapping was next used to measure voltage changes throughout the entire hChaMP structure (Figure 6D through 6G). This allowed for visualization of electrical signal propagation throughout the hChaMP in real time and generation of isochronal maps of activation
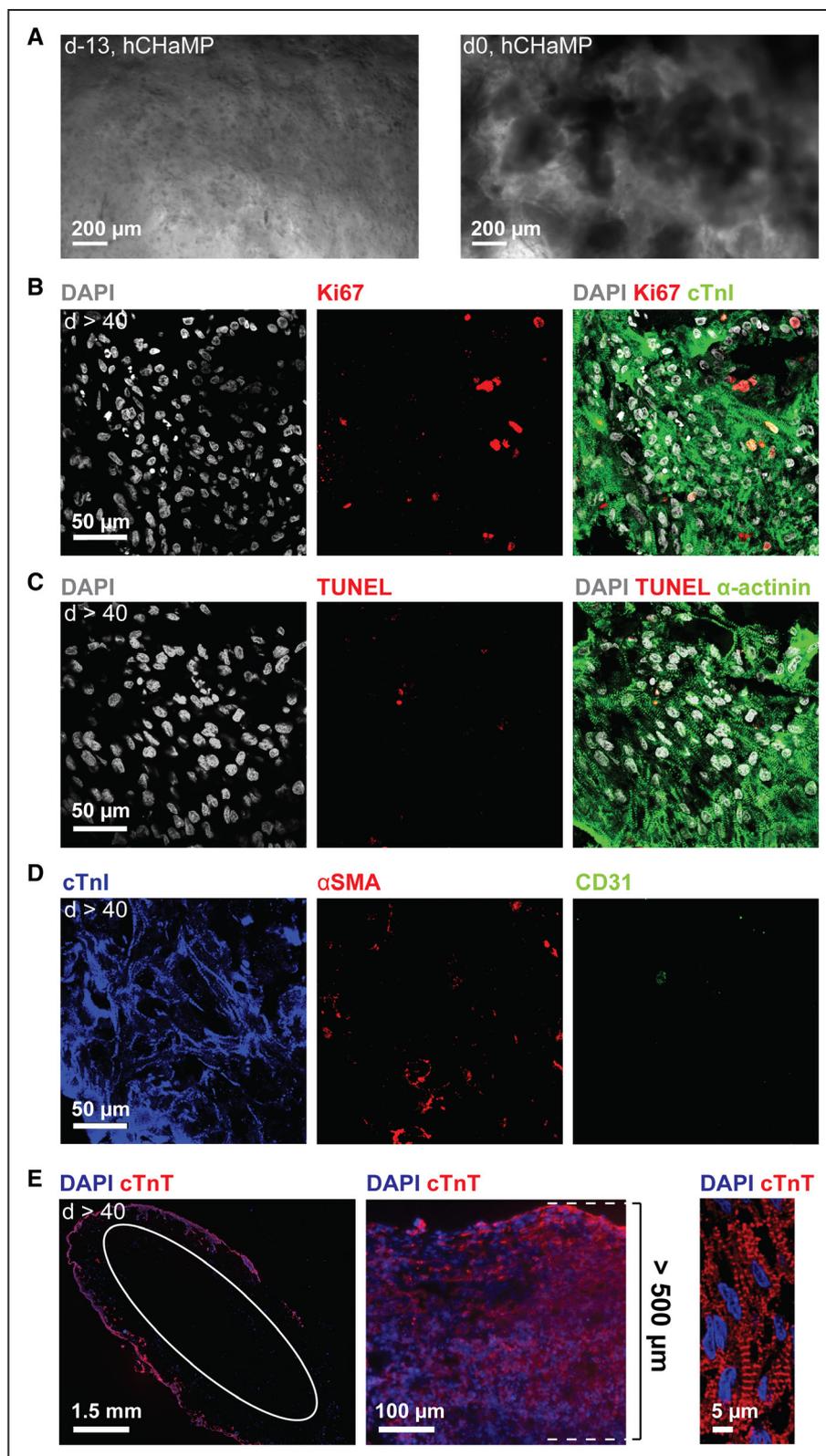
Figure 4. Contiguous muscle formation in human chambered muscle pump (hChaMP) with ongoing proliferation and limited cell death.
A, Single human induced pluripotent cells (hiPSCs; d−13) and hiPSC colonies (d0) in hChaMP. **B–D**, Immunofluorescence staining at 6 wk following lactate treatment. The scale is the same for all images. **B**, Proliferation via Ki67 (nuclear antigen Ki67) staining. **C**, Cell death via terminal deoxynucleotidyl transferase dUTP nick end labeling (TUNEL) staining. **D**, Staining for cardiomyocytes, smooth muscle cells, and endothelial cells in the hChaMP via cTnI (cardiac troponin I), αSMA (alpha-smooth muscle actin), and CD31 (cluster of differentiation 31) staining, respectively. **E**, From **left** to **right**, contiguous muscle formation on the majority of the exterior surface of the hChaMP stained for cTnT (cardiac troponin T; white circle indicates inner wall of chamber cross section), a thick region of the hChaMP wall with muscle depth of 500 µm, and high-magnification image of sarcomeric striations within an hChaMP. DAPI indicates 4′,6-diamidino-2-phenylindole.
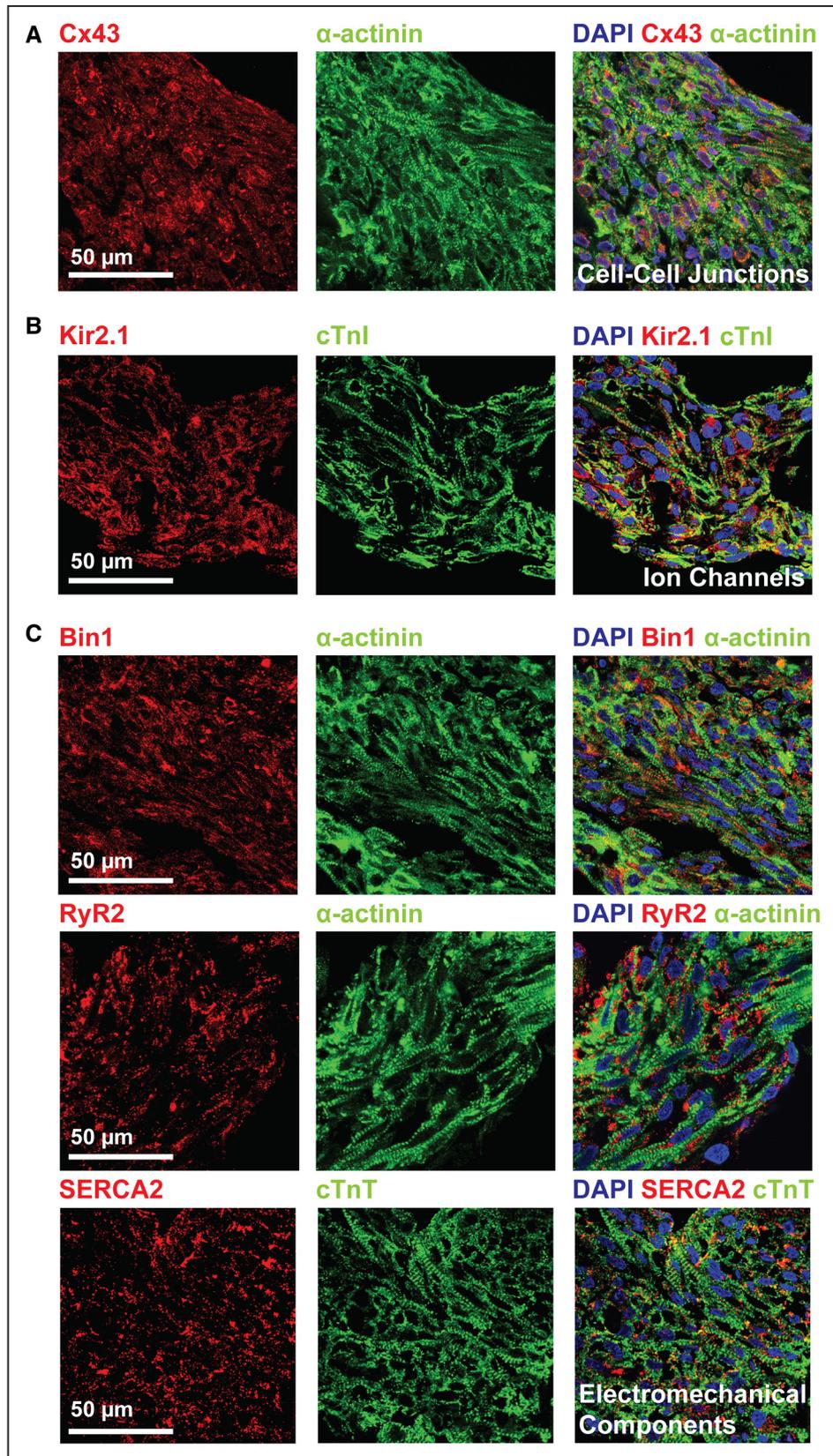
Figure 5. Phenotypic indices of differentiation and maturation of cardiomyocytes of human chambered muscle pumps (hChaMPs).
hChaMPs 6 wk following completion of differentiation and lactate purification protocols were prepared for histological sectioning with subsequent immunolabeling for (**A**) Cx43 (connexin 43), (**B**) Kir2.1, (**C**) Bin1 (bridging integrator-1), RyR2 (ryanodine receptor 2), and SERCA2 (sarcoplasmic reticulum ATPase2a). The scale is the same for all images. CtnI indicates cardiac troponin I; cTnT, cardiac troponin T; and DAPI, 4′,6-diamidino-2-phenylindole.
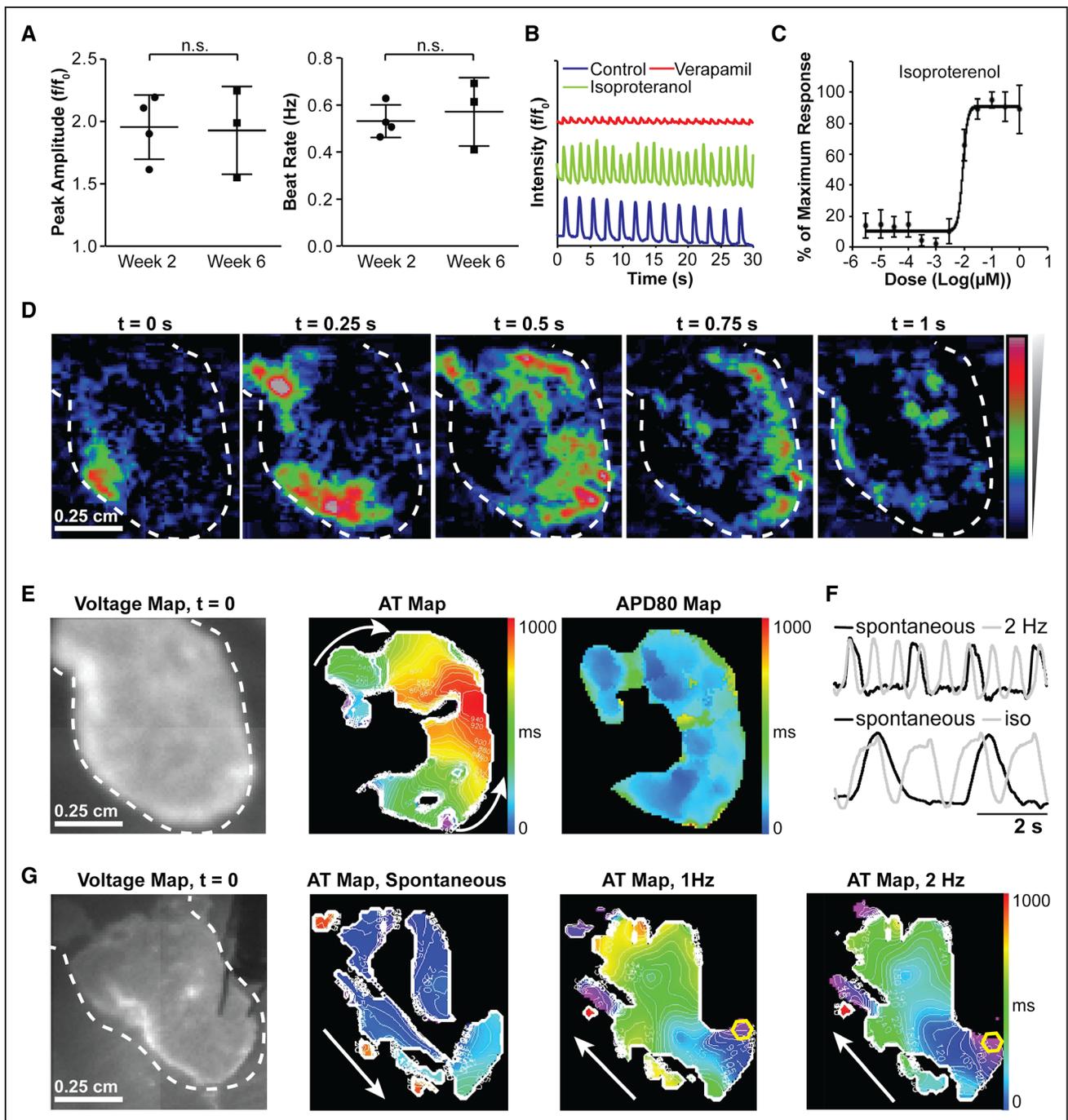
Figure 6. Electrochemical function of human chambered muscle pumps (hChaMPs).
A, Calcium transient activity of hChaMPs at 2 and 6 wk following differentiation. Peak amplitude (**left**) and beat rate (**right**) calculated from calcium peaks; n=4 hChaMPs at week 2, and n=3 hChaMPs at week 6; $P=0.912$ and 0.645 for peak amplitude and beat rate, respectively, Student t test. **B**, Calcium handling response of hChaMPs to pharmacological agents, including isoproterenol (Iso) and verapamil. **C**, Dose-response effect of Iso in hChaMPs, measured by calcium transient activity in terms of beat rate, from 5 different areas across 2 hChaMPs. **E**, Voltage propagation of hChaMP presented as time-sequential images. The scale is the same for all images. **E**, Spontaneous electrical activity of hChaMP including isochronal maps of activation time at 50% of depolarization (AT) and action potential duration at 80% of repolarization (APD80). The scale is the same for all images. **F**, Representative traces for hChaMP with pacing and with exposure to Iso, respectively. **G**, Electrical activity of hChaMP, spontaneous and with pacing at 1 and 2 Hz; white arrows show the direction of propagation, and yellow hexagons show the site of pacing. The scale is the same for all images. n.s. indicates not statistically significant.

time at 50% depolarization, as well as action potential duration at 80% repolarization (Figure 6D and 6E; Movie VI in the Data Supplement). The average spontaneous

action potential duration was 499.9±83.5 ms (n=4), and action potentials detected on the surface of the hChaMP reflected a dramatic and predicted response to altered

pacing frequency and drug stimulation (Figure 6F). In most cases, the electrical activity of the hChaMP began in one area and propagated throughout the structure (Figure 6E). The location of the structure from which the activity was propagated was stochastic, sometimes from the large vessels, sometimes from a region near the large vessels, and sometimes near the apex. This outcome likely reflects the accumulation of pacemaker cells or immature cardiomyocytes with the capacity for spontaneous membrane depolarization in a given region that dominates and, therefore, initiates the response. However, in some cases, the spontaneous source of depolarization could be overcome and the directionality of propagation altered via electrical point stimulation at another location within the hChaMP (Figure 6G; Movies VII and VIII in the Data Supplement). Of note, pacing for less than an hour increased the total area in which action potentials were detected (Figure 6G), suggesting electrical stimulation can promote connectivity and further enhance the concerted function of the hChaMP. In the absence of electrical stimulation, action potentials were detected across 56±28% of the total surface area of the hChaMP (n=4). The locations of detectable electrical signals likely correspond to the distribution of cardiomyocytes throughout the hChaMP, as costaining of calcium dye-treated tissues confirms that electrically active regions are cTnT positive (Figure V in the Data Supplement). Furthermore, optical mapping of acellular hChaMPs was performed to verify the true nature of action potentials observed in cellularized samples (Figure VI in the Data Supplement).

To determine mechanical pump function, hChaMPs were first evaluated for contractile performance, as indicated by beats per minute and rates of contraction and relaxation (Figure 7A and 7B). Contractile performance was not enhanced over time but did not decline significantly either, supporting the long-term health of the hChaMP. Contractility analysis was also used to measure the dose response of hChaMPs to isoproterenol treatment (Figure 7C). This analysis yielded a drug concentration producing 50% of maximum response of 0.009 μM, identical to the value derived from calcium transient analysis. To determine pressure-volume dynamics as a clinically relevant comparator for this new model system, a conductance catheter harboring a pressure transducer was inserted into one chamber of the hChaMP. Beat rate was determined via fast Fourier transform of pressure versus time plots (Figure 7D). The coupling of the pressure transducer with the conductance catheter enabled us to plot both pressure and volume simultaneously as a function of time, which was done for spontaneously contracting and isoproterenol-treated hChaMPs, as well as for an acellular control hChaMP to assess background noise (Figure 7E). Pressure-volume versus time plots were used to generate pressure-volume loops and from these stroke work could be determined despite the fact that there are no valves to resist emptying and filling. The average stroke work calculated from spontaneous loops shown in Figure 7E was 14.5±1.1 nJ. This value was reduced to 4.9±1.6 nJ in the presence of 1 μM isoproterenol. The stroke work value derived from noise fluctuations in the acellular control was 0.26±0.15 nJ. Using the pressure-volume setup, we were able to detect changes in beat rate corresponding to multiple concentrations of isoproterenol (Figure 7F). The usual volume moved through the chambers was 0.5 μL, and maximum volume moved through the chambers was 5.0 μL, which is ≈25% of that of the average stroke volume of an adult murine heart.[34] Based on these values, we calculated an ejection fraction of 0.7% on average, with a maximum value of 6.5% (Figure 7G). These measurements are on par with data shown in single ventricle models.[6,7]

To verify the accuracy of these values and determine the effect of wall cellularization on stroke volume, we developed an in silico finite element model using the hChaMP digital template. Using this model, changes in chamber volume were assessed under 3 different assumptions: (1) the entirety of the wall thickness is occupied by cells, (2) approximately half of the wall thickness (600–650 μm) is occupied by cells, and (3) the cellularization is limited to the outer 200 to 250 μm of the structure (Figure VII in the Data Supplement). Based on the underlying substrate bioink stiffness and the age of cultured hiPSC-derived cardiomyocytes, a maximum contraction stress of 3.5 kPa was prescribed for this model.[35] The stroke volume calculated for the 200 to 250 μm wall thickness (most similar to the level of cellularization we observed) was ≈1.7 μL. The experimentally determined stroke volume is slightly lower than this, likely due to an uneven distribution of cardiomyocytes across the hChaMP surface. Based on the in silico model, we expect that a fully cellularized hChaMP under the same conditions would produce a stroke volume of ≈14 μL, which approaches that of the adult murine heart.[34]

DISCUSSION

In the last decade, cardiac tissue engineering capitalized on robust differentiation protocols for human cardiomyocytes and microfabrication techniques to generate microscale model systems for drug testing. Expansion to macroscale models, where human heart structure and function can be examined on multiple scales, will greatly support medical device testing, preclinical cardiology, and push research closer to clinical transplantation. Still, there are substantial challenges when it comes to recapitulating the cell-cell interactions that are critical to electromechanical function without sacrificing geometric complexity. Here, we take a substantive step toward a macroscale chambered model of the human heart by combining basic scientific discoveries in ECM-stem cell dynamics, technical advances in 3D bioprinting, and lessons learned from human organoid culture.
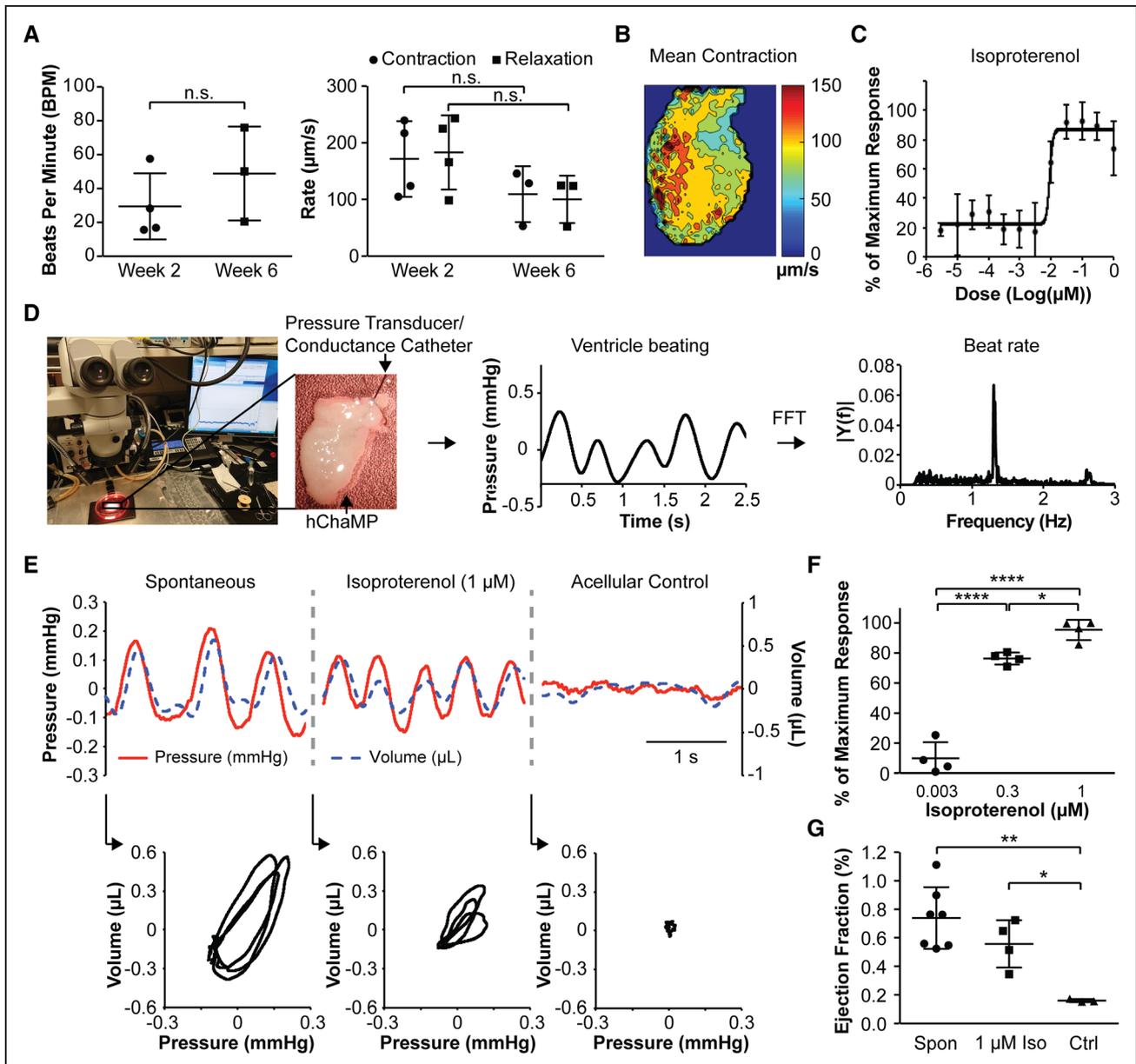
Figure 7. Mechanical function of human chambered muscle pumps (hChaMPs).
A, Contractility in terms of beats per minute of cardiomyocytes of hChaMPs at 2 and 6 wk following differentiation and lactate purification. **Right**, Contractility in terms of rates of contraction and relaxation of cardiomyocytes of hChaMPs at 2 and 6 wk following differentiation and lactate purification. n=4 hChaMPs at week 2, and n=3 hChaMPs at week 6; for beat rate, $P=0.324$, Student t test; for contraction rate, $P=0.235$, Student t test; for relaxation rate, $P=0.229$, Mann-Whitney U test. **B**, A representative map of contractility rate from an hChaMP with spontaneous (Spon) activity. **C**, Dose-response effect of isoproterenol (Iso) in hChaMPs, measured by contractility in terms of beat rate, from at least 3 different areas across 2 hChaMPs. **D**, An overview of the methodology for obtaining interchamber pressure and volume using a pressure transducer coupled to a conductance catheter for obtaining estimates of distance from the catheter to the chamber wall and back-calculating chamber volume. Catheters were threaded through one of the large vessels extending from the top of the hChaMP and placed submerged in a 37°C bath containing culture medium that was mounted on a temperature-controlled heated stage. Catheter readouts were amplified to provide real-time measurement of pressure and volume. FFT (fast Fourier transform) was used to convert pressure vs time associations to beat rates. **E**, Representative traces of pressure and volume dynamics over a 2.5-s interval in hChaMPs with and without Iso, as well as in acellular control (Ctrl) hChaMPs, were used for generating corresponding pressure-volume loops (3 contraction cycles for each condition). **F**, Iso response in terms of beat rate measured by catheters; n=4 hChaMPs per condition. *$P<0.05$, ****$P<0.001$, 1-way ANOVA with Tukey post hoc test. **G**, Ejection fraction of Spon (n=7 hChaMPs), hChaMPs treated with 1 μmol/L Iso (n=4 hChaMPs), and acellular Ctrl hChaMPs (n=3 hChaMPs). *$P<0.05$, **$P<0.01$, 1-way ANOVA with Tukey post hoc test. ns indicates not statistically significant.

Recapitulating Cell-ECM Interactions to Facilitate Proliferation and Differentiation

The ECM-exclusive nature of the bioink means remodeling can occur uninterrupted by synthetic materials. Indeed, the epitopes provided in the bioink engage several integrin heterodimers including α1β1, α2β1, α10β1, α11β1 (collagen), α5β1, αvβ3 (gelatin), α6β1, α7β1, α6β4 (LN-111), α4β1, α5β1, and αvβ3 (FN). Of these, hiPSCs express receptors for all ECM of the bioink, namely α11β1, α5β1, and α6β1.[36] Engagement of hiPSCs to the ECM was favored insofar as it promoted cell viability, pluripotency, and anchorage of growing colonies. Striking a balance between maintenance of pluripotency and initiation of differentiation is challenging in the presence of ECM, as only α6β1 has been reported to promote pluripotency,[37] while all others appear to promote differentiation in an ECM type-specific manner. We attempted to tip the balance in favor of hiPSC proliferation by preincubating the hiPSCs with LN-111 (binds α6β1) before inclusion with remaining components of the bioink. In addition, we utilized high cell densities to allow cell-cell interactions to dominate (though not eliminate) cell-matrix interactions. Also, as colonies grew, it appeared that either ECM hydrolysis or direct remodeling of ECM via MMPs (matrix metalloproteinases) occurred to provide space, as hiPSCs expressed MMPs 1, 5, and 6, where MMP1 is a protease capable of degrading both collagen and gelatin although the substrates of MMP5 and 6 are poorly understood. Over time, other ECM proteins emerged in the hChaMP (Figure VIII in the Data Supplement), most notably type III collagen, which will engage at least integrins α1β1 and α2β1, which are highly expressed in iPSC-derived cardiomyocytes.[38] In addition, iPSC-derived cardiomyocytes express a myriad of MMPs including 1 to 3, 10, 11, 14 to 16, and 19,[38] as do hiPSC-derived smooth muscle cells, which were present, albeit more rarely in the hChaMP. Productive remodeling of a living pump of this type will be critical to improving functional performance and therefore potential as a model system and future therapeutic.

In Situ Differentiation to Enhance Cell Density and Tissue Connectivity

One of the unique approaches taken in this study is that of in situ differentiation. Rather than printing with differentiated hiPSC-cardiomyocytes, which requires breaking up the critical connections these cells form in 2-dimensional culture, we printed with pluripotent stem cells. In developing a bioink that enabled hiPSC proliferation, we were able to achieve high cell densities in the form of large colonies within the tissue before differentiation. We then applied a small molecule−based differentiation protocol to the 3D structures to generate cardiac tissue. This approach is innovative in that it essentially couples the

process of differentiation with the formation of cell connections within the tissue. These nascent connections are able to form as a result of the generation of high densities of hiPSCs colonies before differentiation.[38a] This critical expansion phase enabled final cell densities (≈0.1 mg DNA/g of hChaMP) of the same order of magnitude as native tissue (≈0.3 mg DNA/g of myocardial mass).[32] Using pipetted disks composed of the optimized bioink formulation, we detected that there was, on average, 6.2 μg of DNA in a single disk. Assuming a disk thickness of 1 mm, and taking into account limitations to nutrient diffusion, the resulting thickness of viable tissue area can be estimated to be 200 μm. If the average cell contains 6 pg of DNA, we can estimate the final cell density in the viable region of the disk to be a little over 100 million cells/cm^3. Given that the starting concentration of hiPSCs was 15 million cells/mL, the final cell density we achieved is >500% higher than the starting density. In the context of the hChaMP, this increase in cell density resulted in a cardiac muscle thickness of between 100 and 500 μm. Wall thicknesses on the low end of this spectrum match what has been previously demonstrated in the literature, and the high end of the spectrum far exceeds existing tissue models.[6–8]

Advances to the Field

While multiple groups have generated variations on tissue-engineered ventricles and whole heart models, the hChaMP is the first to achieve robust electromechanical function in a perfusable, chambered cardiac pump. Notably, we show that the hChaMP can maintain these functions for at least 6 weeks, while most similar models have been characterized only up to 2 weeks after fabrication.[6–8,18] The functional readouts we assess are on par with, if not better than, values reported in the literature for similar models. This study is only 1 of 3 to measure pressure-volume dynamics within a tissue-engineered chamber model, and the pressure generated by the hChaMP, while low (0.23 mm Hg), is higher than other reported values.[6,7] Stroke work and ejection fraction are on par with existing systems, and similar to results reported by MacQueen et al,[7] we show that the hChaMP can respond to a range of isoproterenol doses. Furthermore, the hChaMP exceeds existing models in wall thickness. The lowest muscularized wall thicknesses observed (≈100 μm) match what has been shown in single ventricle models. However, at its thickest regions, we show that the muscularized region can exceed 500 μm, which is much higher than any reported values in the literature. Viable cells were localized to the outside of the structure, but given the perfusability of our model, we anticipate that internal cell viability and resulting wall thickness will only increase with further improvements to culture protocols. Furthermore, as our in silico model demonstrated, increasing the cell layer

thickness should increase the volume output of the hChaMP, resulting in more robust pump function (Figure VII in the Data Supplement).

We hypothesize that the robust function and tissue density we have observed is due to the novel in situ differentiation approach, which allows nascent cardiac cells to differentiate while forming undisrupted connections to each other in a 3D environment, similar to what would occur during development. That we were able to accomplish this in a bioink that is also amenable to 3D printing complex geometries allowed us to generate an unprecedented perfusable pump model.

Future Considerations

The next steps toward improving upon this model will include efforts to increase the thickness, homogeneity, and organization of the muscle wall, as well as to spur maturation of individual cardiac muscle cells.

Improving Tissue Thickness

Increased muscle thickness will improve pump function and prevent rupture. One approach for enabling thick tissue cultivation is to introduce convective flow in a bioreactor system.[39,40] While we did introduce convection to the hChaMP via rocking, due to its complex geometry, a perfusion bioreactor would be practically necessary to ensure adequate flow through the chambers and to mimic physiological conditions more precisely. Perfusion bioreactors are capable of recapitulating pulsatile flow profiles and, combined with mechanical and electrical stimulation, enable recellularized cardiac ECM constructs to achieve the cell density of native myocardium.[41,42] Given this consideration, together with the fact that cardiac biomechanics are continually changing not only during the contraction cycle but also by developmental stage,[43] an optimized dynamic culture protocol with time-variant properties over both long and short time scales conducted by a perfusion bioreactor could be used for further improving tissue robustness and physiological functions of the hChaMP.

In addition to manipulating the external culture system, another approach for increasing tissue thickness is to maintain nutrient and oxygen supply within the engineered tissue by means of a well-developed vascular network; this can be achieved through incorporation of endothelial cells or the use of sacrificial materials to 3D print vascular lumen.[44–49] In the current study, endothelial differentiation and tube formation were not intentionally included, but future design iterations should include stimulants of endothelial differentiation and vascular network formation.

Improving Tissue Maturation

In addition to enhancing the thickness of the cardiac muscle within the hChaMP, improvement of this model will require enhanced maturation of cardiomyocytes and

corresponding pump function. Here, we have shown the expression of maturation markers associated with cell-cell junctions, ion handling, and excitation-contraction coupling, but mature cell alignment and sarcomeric organization are still lacking. Furthermore, in addition to structural organization, multiple metrics of functional maturation should also be met to augment the performance of a living pump.

Electrical stimulation has been shown to improve ion handling, action potential propagation, cell alignment, and structural maturation in 3D tissues made of stem cell–derived cardiomyocytes.[50] Furthermore, by combining field stimulation with mechanical loading, researchers have generated 3D tissues with neonatal rat cardiomyocytes that demonstrate a positive force-frequency response, a critical characteristic of native cardiac tissue.[4] In another case, researchers imposed controlled afterload on hiPSC-derived cardiac tissues, which subsequently exhibited a positive Frank-Starling relationship.[5] Hence, we hypothesize that introducing electromechanical conditioning to the hChaMP will significantly improve maturation and resulting function. In addition, with some modifications and improvements, the hChaMP provides a unique system to investigate the characteristic Frank-Starling relationship of the native heart. While in vitro assessment of this relationship in most tissue-engineered constructs is based on length versus resulting force of contraction, physiologically it is a metric that relates stroke volume to the end-diastolic volume. A tissue-engineered construct that can hold volume is, therefore, necessary to recapitulate this relationship.[7] The main limitation to achieving this with the hChaMP is the lack of valvular structures, which precludes the generation of a controlled preload. A perfusion bioreactor that incorporates valves[7] would allow for pressure buildup within the hChaMP, as well as control over fill volume of the construct. Synchronized with field stimulation, such a system would allow for electromechanical conditioning to promote maturation, generation of more physiological pressure-volume loops, and the capacity to measure the Frank-Starling relationship based on stroke volume and preload. In the short term, the most feasible avenue to achieve this end would be the incorporation of mechanical valves into tubing that attaches to the vessel inlet and outlets. In the future, we can explore the possibility of tissue-engineered valves, which would enable the generation of 4-chambered structures with valves for both atrial and ventricular filling.

Finally, there are a myriad of soluble factors that have been explored to promote cardiomyocyte maturation. Among these are the hormone tri-iodo-L-thyronine,[51] the alpha-adrenergic agonist phenylephrine,[52] and insulin-like growth factor.[53,54] MicroRNAs have also been shown to play a key role in driving metabolic maturation of stem cell–derived cardiomyocytes.[55,56] Incorporation of soluble signals along with electrical and physical cues could

provide an avenue to further mature cardiomyocytes of the hChaMP.

Versatility and Applicability of Bioink

To generate the hChaMP, we utilized extrusion-based printing of an ECM-based bioink into a gelatin support bath. However, because of the photo-crosslinkable nature of the bioink, it is compatible with other 3D fabrication modalities, including casting and photolithography-based printing. Initially, due to the low viscosity of the bioink, we developed an approach that involved printing an inverted model with a sacrificial material and backfilling with cell-laden ink (Figure IIA in the Data Supplement). While this method could reproducibly generate structures with intact chambers, we ultimately found that the use of the sacrificial material was not conducive to hiPSC viability and proliferation (Figure IIB through IIE in the Data Supplement). However, it is likely that this methodology could still be used to 3D printed tissues using cell types that are less sensitive than hiPSCs or the sacrificial material could be modified to improve resultant cell health.

In addition to versatility of fabrication processes, the bioink components could theoretically be tailored to the needs of a variety of cell types. The structural integrity of the hChaMP is due to the photo-crosslinkable methacrylate groups on the GelMA and ColMA, but we also entrapped noncrosslinkable ECM proteins (FN and LN). While these soluble proteins slightly increased the viscosity of the bioink, the majority of their benefit came from improving cardiac differentiation outcomes (Table). One could theoretically alter the ECM makeup of the ink without sacrificing structural integrity to better promote differentiation to another lineage. Hence, this bioink is a versatile tool for fabricating a myriad of engineered tissues.

Conclusions

In summary, this work is the first to realize macroscale beating function in a geometrically complex and perfusable chambered structure. This important outcome was made possible by an optimized bioink that allowed extensive stem cell proliferation before differentiation to yield contiguous muscle walls of up to 500 µm in thickness. This approach could be applied to many other cell types with poor proliferative and migratory capacity following differentiation. In the end, the living human pump shown here and future design iterations will find utility for multiscale in vitro cardiology assays, injury and disease modeling, medical device testing, and regenerative medicine research that should more easily transfer to clinically relevant outcomes.

REFERENCES

1. Eschenhagen T, Fink C, Remmers U, Scholz H, Wattchow J, Weil J, Zimmermann W, Dohmen HH, Schäfer H, Bishopric N, et al. Three-dimensional reconstitution of embryonic cardiomyocytes in a collagen matrix: a new heart muscle model system. *FASEB J*. 1997;11:683–694. doi: 10.1096/fasebj.11.8.9240969

ORIGINAL RESEARCH

2. Zimmermann WH, Fink C, Kralisch D, Remmers U, Weil J, Eschenhagen T. Three-dimensional engineered heart tissue from neonatal rat cardiac myocytes. *Biotechnol Bioeng*. 2000;68:106–114.

3. Zimmermann WH, Schneiderbanger K, Schubert P, Didié M, Münzel F, Heubach JF, Kostin S, Neuhuber WL, Eschenhagen T. Tissue engineering of a differentiated cardiac muscle construct. *Circ Res*. 2002;90:223–230. doi: 10.1161/hh0202.103644

4. Godier-Furnémont AF, Tiburcy M, Wagner E, Dewenter M, Lämmle S, El-Armouche A, Lehnart SE, Vunjak-Novakovic G, Zimmermann WH. Physiologic force-frequency response in engineered heart muscle by electromechanical stimulation. *Biomaterials*. 2015;60:82–91. doi: 10.1016/j.biomaterials.2015.03.055

5. Leonard A, Bertero A, Powers JD, Beussman KM, Bhandari S, Regnier M, Murry CE, Sniadecki NJ. Afterload promotes maturation of human induced pluripotent stem cell derived cardiomyocytes in engineered heart tissues. *J Mol Cell Cardiol*. 2018;118:147–158. doi: 10.1016/j.yjmcc.2018.03.016

6. Li RA, Keung W, Cashman TJ, Backeris PC, Johnson BV, Bardot ES, Wong AOT, Chan PKW, Chan CWY, Costa KD. Bioengineering an electro-mechanically functional miniature ventricular heart chamber from human pluripotent stem cells. *Biomaterials*. 2018;163:116–127. doi: 10.1016/j.biomaterials.2018.02.024

7. MacQueen LA, Sheehy SP, Chantre CO, Zimmerman JF, Pasqualini FS, Liu X, Goss JA, Campbell PH, Gonzalez GM, Park SJ, et al. A tissue-engineered scale model of the heart ventricle. *Nat Biomed Eng*. 2018;2:930–941. doi: 10.1038/s41551-018-0271-5

8. Lee A, Hudson AR, Shiwarski DJ, Tashman JW, Hinton TJ, Yerneni S, Bliley JM, Campbell PG, Feinberg AW. 3D bioprinting of collagen to rebuild components of the human heart. *Science*. 2019;365:482–487. doi: 10.1126/science.aav9051

9. Hinton TJ, Jallerat Q, Palchesko RN, Park JH, Grodzicki MS, Shue HJ, Ramadan MH, Hudson AR, Feinberg AW. Three-dimensional printing of complex biological structures by freeform reversible embedding of suspended hydrogels. *Sci Adv*. 2015;1:e1500758. doi: 10.1126/sciadv.1500758

10. Bejleri D, Streeter BW, Nachlas ALY, Brown ME, Gaetani R, Christman KL, Davis ME. A bioprinted cardiac patch composed of cardiac-specific extracellular matrix and progenitor cells for heart repair. *Adv Healthc Mater*. 2018;7:e1800672. doi: 10.1002/adhm.201800672

11. Hermsen JL, Burke TM, Seslar SP, Owens DS, Ripley BA, Mokadam NA, Verrier ED. Scan, plan, print, practice, perform: development and use of a patient-specific 3-dimensional printed model in adult cardiac surgery. *J Thorac Cardiovasc Surg*. 2017;153:132–140. doi: 10.1016/j.jtcvs.2016.08.007

12. Hinton TJ, Hudson A, Pusch K, Lee A, Feinberg AW. 3D Printing PDMS elastomer in a hydrophilic support bath via freeform reversible embedding. *ACS Biomater Sci Eng*. 2016;2:1781–1786. doi: 10.1021/acsbiomaterials.6b00170

13. Ripley B, Kelil T, Cheezum MK, Goncalves A, Di Carli MF, Rybicki FJ, Steigner M, Mitsouras D, Blankstein R. 3D printing based on cardiac CT assists anatomic visualization prior to transcatheter aortic valve replacement. *J Cardiovasc Comput Tomogr*. 2016;10:28–36. doi: 10.1016/j.jcct.2015.12.004

14. Vukicevic M, Mosadegh B, Min JK, Little SH. Cardiac 3D printing and its future directions. *JACC Cardiovasc Imaging*. 2017;10:171–184. doi: 10.1016/j.jcmg.2016.12.001

15. Wang L, Xu C, Zhu Y, Yu Y, Sun N, Zhang X, Feng K, Qin J. Human induced pluripotent stem cell-derived beating cardiac tissues on paper. *Lab Chip*. 2015;15:4283–4290. doi: 10.1039/c5lc00919g

16. Yoo SJ, Thabit O, Kim EK, Ide H, Yim D, Dragulescu A, Seed M, Grosse-Wortmann L, van Arsdell G. 3D printing in medicine of congenital heart diseases. *3D Print Med*. 2015;2:3. doi: 10.1186/s41205-016-0004-x

17. Edri R, Gal I, Noor N, Harel T, Fleischer S, Adadi N, Green O, Shabat D, Heller L, Shapira A, et al. Personalized hydrogels for engineering diverse fully autologous tissue implants. *Adv Mater*. 2019;31:e1803895. doi: 10.1002/adma.201803895

18. Noor N, Shapira A, Edri R, Gal I, Wertheim L, Dvir T. 3D Printing of personalized thick and perfusable cardiac patches and hearts. *Adv Sci (Weinh)*. 2019;6:1900344. doi: 10.1002/advs.201900344

19. Costa-Silva B, da Costa MC, Melo FR, Neves CM, Alvarez-Silva M, Calloni GW, Trentin AG. Fibronectin promotes differentiation of neural crest progenitors endowed with smooth muscle cell potential. *Exp Cell Res*. 2009;315:955–967. doi: 10.1016/j.yexcr.2009.01.015

20. Wong JC, Gao SY, Lees JG, Best MB, Wang R, Tuch BE. Definitive endoderm derived from human embryonic stem cells highly express the integrin receptors alphaV and beta5. *Cell Adh Migr*. 2010;4:39–45. doi: 10.4161/cam.4.1.10627

21. Brafman DA, Phung C, Kumar N, Willert K. Regulation of endodermal differentiation of human embryonic stem cells through integrin-ECM interactions. *Cell Death Differ*. 2013;20:369–381. doi: 10.1038/cdd.2012.138

22. Narayanan K, Lim VY, Shen J, Tan ZW, Rajendran D, Luo SC, Gao S, Wan AC, Ying JY. Extracellular matrix-mediated differentiation of human embryonic stem cells: differentiation to insulin-secreting beta cells. *Tissue Eng Part A*. 2014;20:424–433. doi: 10.1089/ten.TEA.2013.0257

23. Li Y, Gautam A, Yang J, Qiu L, Melkoumian Z, Weber J, Telukuntla L, Srivastava R, Whiteley EM, Brandenberger R. Differentiation of oligodendrocyte progenitor cells from human embryonic stem cells on vitronectin-derived synthetic peptide acrylate surface. *Stem Cells Dev*. 2013;22:1497–1505. doi: 10.1089/scd.2012.0508

24. Caiazzo M, Okawa Y, Ranga A, Piersigilli A, Tabata Y, Lutolf MP. Defined three-dimensional microenvironments boost induction of pluripotency. *Nat Mater*. 2016;15:344–352. doi: 10.1038/nmat4536

25. Derda R, Musah S, Orner BP, Klim JR, Li L, Kiessling LL. High-throughput discovery of synthetic surfaces that support proliferation of pluripotent cells. *J Am Chem Soc*. 2010;132:1289–1295. doi: 10.1021/ja906089g

26. Tan TW, Huang YL, Chang JT, Lin JJ, Fong YC, Kuo CC, Tsai CH, Chen YJ, Hsu HC, Cho DY, et al. CCN3 increases BMP-4 expression and bone mineralization in osteoblasts. *J Cell Physiol*. 2012;227:2531–2541. doi: 10.1002/jcp.22991

27. Saidak Z, Le Henaff C, Azzi S, Marty C, Da Nascimento S, Sonnet P, Marie PJ. Wnt/β-catenin signaling mediates osteoblast differentiation triggered by peptide-induced α5β1 integrin priming in mesenchymal skeletal cells. *J Biol Chem*. 2015;290:6903–6912. doi: 10.1074/jbc.M114.621219

28. Dzobo K, Vogelsang M, Parker MI. Wnt/beta-catenin and mek-erk signaling are required for fibroblast-derived extracellular matrix-mediated endoderm differentiation of embryonic stem cells. *Stem Cell Rev*. 2015;11:761–773

29. Cheng P, Andersen P, Hassel D, Kaynak BL, Limphong P, Juergensen L, Kwon C, Srivastava D. Fibronectin mediates mesendodermal cell fate decisions. *Development*. 2013;140:2587–2596. doi: 10.1242/dev.089052

30. Jung JP, Hu D, Domian IJ, Ogle BM. An integrated statistical model for enhanced murine cardiomyocyte differentiation via optimized engagement of 3D extracellular matrices. *Sci Rep*. 2015;5:18705. doi: 10.1038/srep18705

31. Majkut S, Idema T, Swift J, Krieger C, Liu A, Discher DE. Heart-specific stiffening in early embryos parallels matrix and myosin expression to optimize beating. *Curr Biol*. 2013;23:2434–2439. doi: 10.1016/j.cub.2013.10.057

32. Adler CP, Friedburg H, Herget GW, Neuburger M, Schwalb H. Variability of cardiomyocyte DNA content, ploidy level and nuclear number in mammalian hearts. *Virchows Arch*. 1996;429:159–164. doi: 10.1007/bf00192438

33. Harding SE, Ali NN, Brito-Martins M, Gorelik J. The human embryonic stem cell-derived cardiomyocyte as a pharmacological model. *Pharmacol Ther*. 2007;113:341–353. doi: 10.1016/j.pharmthera.2006.08.008

34. Lujan HL, DiCarlo SE. Cardiac output, at rest and during exercise, before and during myocardial ischemia, reperfusion, and infarction in conscious mice. *Am J Physiol Regul Integr Comp Physiol*. 2013;304:R286–R295. doi: 10.1152/ajpregu.00517.2012

35. Wheelwright M, Win Z, Mikkila JL, Amen KY, Alford PW, Metzger JM. Investigation of human iPSC-derived cardiac myocyte functional maturation by single cell traction force microscopy. *PLoS One*. 2018;13:e0194909. doi: 10.1371/journal.pone.0194909

36. Messmer T, von Meyenn F, Savino A, Santos F, Mohammed H, Lun ATL, Marioni JC, Reik W. Transcriptional heterogeneity in naive and primed human pluripotent stem cells at single-cell resolution. *Cell Rep*. 2019;26:815–824. e4. doi: 10.1016/j.celrep.2018.12.099

37. Villa-Diaz LG, Kim JK, Laperle A, Palecek SP, Krebsbach PH. Inhibition of focal adhesion kinase signaling by integrin α6β1 supports human pluripotent stem cell self-renewal. *Stem Cells*. 2016;34:1753–1764. doi: 10.1002/stem.2349

38. Churko JM, Garg P, Treutlein B, Venkatasubramanian M, Wu H, Lee J, Wessells QN, Chen SY, Chen WY, Chetal K, et al. Defining human cardiac transcription factor hierarchies using integrated single-cell heterogeneity analysis. *Nat Commun*. 2018;9:4906. doi: 10.1038/s41467-018-07333-4

38a. Kerscher P, Turnbull IC, Hodge AJ, Kim J, Seliktar D, Easley CJ, Costa KD, Lipke EA. Direct hydrogel encapsulation of pluripotent stem cells enables ontomimetic differentiation and growth of engineered human heart tissues. *Biomaterials*. 2016;83:383–395. https://doi.org/10.1016/j.biomaterials.2015.12.011

39. Shadrin IY, Allen BW, Qian Y, Jackman CP, Carlson AL, Juhas ME, Bursac N. Cardiopatch platform enables maturation and scale-up of human pluripotent stem cell-derived engineered heart tissues. *Nat Commun*. 2017;8:1825. doi: 10.1038/s41467-017-01946-x

40. Fortier GM, Gauvin R, Proulx M, Vallée M, Fradette J. Dynamic culture induces a cell type-dependent response impacting on the thickness of

engineered connective tissues. *J Tissue Eng Regen Med*. 2013;7:292–301. doi: 10.1002/term.522

41. Ott HC, Matthiesen TS, Goh SK, Black LD, Kren SM, Netoff TI, Taylor DA. Perfusion-decellularized matrix: using nature's platform to engineer a bioartificial heart. *Nat Med*. 2008;14:213–221. doi: 10.1038/nm1684

42. Sarig U, Nguyen EB, Wang Y, Ting S, Bronshtein T, Sarig H, Dahan N, Gvirtz M, Reuveny S, Oh SK, et al. Pushing the envelope in tissue engineering: ex vivo production of thick vascularized cardiac extracellular matrix constructs. *Tissue Eng Part A*. 2015;21:1507–1519. doi: 10.1089/ten.tea.2014.0477

43. Domian IJ, Yu H, Mittal N. On materials for cardiac tissue engineering. *Adv Healthc Mater*. 2017;6:1600768. doi: 10.1002/adhm.201600768

44. Stevens KR, Kreutziger KL, Dupras SK, Korte FS, Regnier M, Muskheli V, Nourse MB, Bendixen K, Reinecke H, Murry CE. Physiological function and transplantation of scaffold-free and vascularized human cardiac muscle tissue. *Proc Natl Acad Sci USA*. 2009;106:16568–16573. doi: 10.1073/pnas.0908381106

45. Masumoto H, Nakane T, Tinney JP, Yuan F, Ye F, Kowalski WJ, Minakata K, Sakata R, Yamashita JK, Keller BB. The myocardial regenerative potential of three-dimensional engineered cardiac tissues composed of multiple human iPS cell-derived cardiovascular cell lineages. *Sci Rep*. 2016;6:29933. doi: 10.1038/srep29933

46. Sekine H, Shimizu T, Sakaguchi K, Dobashi I, Wada M, Yamato M, Kobayashi E, Umezu M, Okano T. In vitro fabrication of functional three-dimensional tissues with perfusable blood vessels. *Nat Commun*. 2013;4:1399. doi: 10.1038/ncomms2406

47. Kang HW, Lee SJ, Ko IK, Kengla C, Yoo JJ, Atala A. A 3D bioprinting system to produce human-scale tissue constructs with structural integrity. *Nat Biotechnol*. 2016;34:312–319. doi: 10.1038/nbt.3413

48. Kolesky DB, Homan KA, Skylar-Scott MA, Lewis JA. Three-dimensional bioprinting of thick vascularized tissues. *Proc Natl Acad Sci USA*. 2016;113:3179–3184. doi: 10.1073/pnas.1521342113

49. Skylar-Scott MA, Uzel SGM, Nam LL, Ahrens JH, Truby RL, Damaraju S, Lewis JA. Biomanufacturing of organ-specific tissues with high cellular density and embedded vascular channels. *Sci Adv*. 2019;5:eaaw2459. doi: 10.1126/sciadv.aaw2459

50. Nunes SS, Miklas JW, Liu J, Aschar-Sobbi R, Xiao Y, Zhang B, Jiang J, Massé S, Gagliardi M, Hsieh A, et al. Biowire: a platform for maturation of human pluripotent stem cell-derived cardiomyocytes. *Nat Methods*. 2013;10:781–787. doi: 10.1038/nmeth.2524

51. Yang X, Rodriguez M, Pabon L, Fischer KA, Reinecke H, Regnier M, Sniadecki NJ, Ruohola-Baker H, Murry CE. Tri-iodo-l-thyronine promotes the maturation

52. Földes G, Mioulane M, Wright JS, Liu AQ, Novak P, Merkely B, Gorelik J, Schneider MD, Ali NN, Harding SE. Modulation of human embryonic stem cell-derived cardiomyocyte growth: a testbed for studying human cardiac hypertrophy? *J Mol Cell Cardiol*. 2011;50:367–376. doi: 10.1016/j.yjmcc.2010.10.029

53. Ito H, Hiroe M, Hirata Y, Tsujino M, Adachi S, Shichiri M, Koike A, Nogami A, Marumo F. Insulin-like growth factor-I induces hypertrophy with enhanced expression of muscle specific genes in cultured rat cardiomyocytes. *Circulation*. 1993;87:1715–1721. doi: 10.1161/01.cir.87.5.1715

54. Montessuit C, Palma T, Viglino C, Pellieux C, Lerch R. Effects of insulin-like growth factor-I on the maturation of metabolism in neonatal rat cardiomyocytes. *Pflugers Arch*. 2006;452:380–386. doi: 10.1007/s00424-006-0059-4

55. Kuppusamy KT, Jones DC, Sperber H, Madan A, Fischer KA, Rodriguez ML, Pabon L, Zhu WZ, Tulloch NL, Yang X, et al. Let-7 family of microRNA is required for maturation and adult-like metabolism in stem cell-derived cardiomyocytes. *Proc Natl Acad Sci USA*. 2015;112:E2785–E2794. doi: 10.1073/pnas.1424042112

56. Lee DS, Chen JH, Lundy DJ, Liu CH, Hwang SM, Pabon L, Shieh RC, Chen CC, Wu SN, Yan YT, et al. Defined microRNAs induce aspects of maturation in mouse and human embryonic-stem-cell-derived cardiomyocytes. *Cell Rep*. 2015;12:1960–1967. doi: 10.1016/j.celrep.2015.08.042

57. Zhu W, Zhao M, Mattapally S, Chen S, Zhang J. CCND2 overexpression enhances the regenerative potency of human induced pluripotent stem cell-derived cardiomyocytes: remuscularization of injured ventricle. *Circ Res*. 2018;122:88–96. doi: 10.1161/CIRCRESAHA.117.311504

58. Mironov S, Jalife J, Tolkacheva EG. Role of conduction velocity restitution and short-term memory in the development of action potential duration alternans in isolated rabbit hearts. *Circulation*. 2008;118:17–25. doi: 10.1161/CIRCULATIONAHA.107.737254

59. Huebsch N, Loskill P, Mandegar MA, Marks NC, Sheehan AS, Ma Z, Mathur A, Nguyen TN, Yoo JC, Judge LM, et al. Automated video-based analysis of contractility and calcium flux in human-induced pluripotent stem cell-derived cardiomyocytes cultured over different spatial scales. *Tissue Eng Part C Methods*. 2015;21:467–479. doi: 10.1089/ten.TEC.2014.0283

60. Updegrove A, Wilson NM, Merkow J, Lan H, Marsden AL, Shadden SC. SimVascular: an open source pipeline for cardiovascular simulation. *Ann Biomed Eng*. 2017;45:525–541. doi: 10.1007/s10439-016-1762-8

61. Maas SA, Ellis BJ, Ateshian GA, Weiss JA. FEBio: finite elements for biomechanics. *J Biomech Eng*. 2012;134:011005. doi: 10.1115/1.4005694